

# Controllable magnetic 3D nitrogen-doped graphene gel: Synthesis, characterization, and catalytic performance



Bowei Wang<sup>a,b</sup>, Leilei Si<sup>a</sup>, Jiyu Geng<sup>a</sup>, Yuhan Su<sup>a</sup>, Yang Li<sup>a,b,c</sup>, Xilong Yan<sup>a,b,c,\*</sup>, Ligong Chen<sup>a,b,c,\*</sup>

<sup>a</sup> School of Chemical Engineering and Technology, Tianjin University, Tianjin, 300350, PR China

<sup>b</sup> Collaborative Innovation Center of Chemical Science and Engineering (Tianjin), Tianjin, 300072, PR China

<sup>c</sup> Tianjin Engineering Research Center of Functional Fine Chemicals, Tianjin, PR China

## ARTICLE INFO

### Article history:

Received 16 August 2016

Received in revised form

20 November 2016

Accepted 21 November 2016

Available online 22 November 2016

### Keywords:

N-doped graphene

Self-assembly

Magnetism

*In situ* synthesis

Gel

## ABSTRACT

Magnetic 3D nitrogen doped graphene gels (MNG) were easily obtained via one-pot hydrothermal synthesis process. It was found that N doping process, reduction of graphene oxide and  $\text{Fe}_3\text{O}_4$  nanoparticles (NPs) generation *in situ* proceeded simultaneously, accompanied by the three-dimensional self-assembly. The MNG hybrids were confirmed to be interconnected porous frameworks of graphene sheets with uniform dispersion of  $\text{Fe}_3\text{O}_4$  NPs embedded or encapsulated in N-doped graphene layers. The catalytic performance of MNG nanocatalysts was evaluated by the reduction of 4-nitrophenol to 4-aminophenol. It was worth noting that the catalytic activity of MNG hybrids was remarkably enhanced by  $\text{Fe}_3\text{O}_4$  NPs loading due to the change of N doping mode induced by the *in situ* synthesis of these magnetic NPs, which did not alter the C/N mass ratio in fact. Meanwhile, the reaction no longer simply followed the pseudo-zero-order kinetics in late stage, this might be attributed to the enhancement of catalytic activity. Furthermore, MNG nanocatalysts were easily recycled by virtue of their superparamagnetism and exhibited excellent stability.

© 2016 Elsevier B.V. All rights reserved.

## 1. Introduction

Doping carbon nanomaterials with heteroatoms have become more and more significant in both chemistry and materials science. Among them, nitrogen atoms, having a comparable atomic size and five valence electrons for bonding, can introduce local high positive charge density and high spin density to their *ortho*-carbon atoms on N-doped graphene (NG) sheets, leading to more metallic-like properties [1,2]. So there is a growing interest among researchers in NG area [3–7]. According to reports, there are four N species on NG: pyridinic N, amino N, pyrrolic N, and graphitic N [8–10].

Because 4-nitrophenol (Nip) is one of the most extensive phenolic pollutants which are quite recalcitrant to degradation in waste water, the reduction of Nip to 4-aminophenol (Amp) by sodium borohydride ( $\text{NaBH}_4$ ) is much more concerned day by day [11]. Although previous report has shown that doping nitrogen atoms can enhance the ability of their *ortho*-carbon atoms to adsorb Nip ions, the carbon atoms next to amino N and graphitic N exhibited

much lower adsorption energy of Nip ions than those next to pyridinic N and pyrrolic N [12]. Thus, we speculate that the catalytic activity of graphene doped with amino N and graphitic N may be higher than the others. It is needful to raise the content of amino N and graphitic N under the same N doping amount, especially the graphitic N which could activate more *ortho*-carbon atoms on NG sheet. However, the preparation of NG is too complicated to control N doping mode, and normally requires a thermal treatment at high temperature [13,14]. For hydrothermal synthesis in particular, which has obvious advantages such as mild reaction conditions and scale-up synthesis [8,15], but so far there is no efficient method available to achieve the target.

In recent years, there exists an increasing interest in the use of three-dimensional (3D) graphene networks, which not only preserve the high specific surface area and electronical conductivity of two-dimensional (2D) plate-like structure, but also possess suitable pore network as well as multidimensional electron transport pathways [8,16–18]. Thereinto, magnetic 3D graphene gels have drawn more attention due to easier recycling and excellent performance, which is crucial for cost-effective industrial process [19–21]. Meanwhile, many 3D graphene gels have been successfully used to catalytic reduction of Nip to Amp by  $\text{NaBH}_4$ . However, most of them support metal nanoparticles (NPs) of Au, Pd, etc [22,23]. Although

\* Corresponding authors at: School of Chemical Engineering and Technology, Tianjin University, Tianjin, 300350, PR China.

E-mail addresses: [yan@tju.edu.cn](mailto:yan@tju.edu.cn) (X. Yan), [lgchen@tju.edu.cn](mailto:lgchen@tju.edu.cn) (L. Chen).

precious metal catalysts have shown nice catalytic performance in many reactions [24–32], the exorbitant price and scarce supply of them always limit their practical application. From the aspect of green chemistry, more economical and environmentally friendly alternatives, such as metal free and/or earth-abundant non-noble metal-based catalysts, are still desired. Magnetic 3D nitrogen doped graphene gel (MNG) is indeed a good choice, which is highly catalytic activity, economical, and environmental protection [33,34]. Nevertheless, there are few reports on the reduction of Nip to Amp by  $\text{NaBH}_4$  over this kind of catalysts, not to mention the control of N doping mode during the preparation process of such materials.

In this work, we tried to establish a green and mild method to regulate the N doping mode on graphene instead of conventional thermal treatment at high temperature and/or tedious alteration of N source. Specifically, we attempted to control the N doping mode by using the interaction between iron salt and ethylenediamine in the hydrothermal synthetic process of MNG hybrids. Thus, the process of endowing NG with the magnetism, the regulation of N doping mode, and the three-dimensional self-assembly could be finished at the same time during the hydrothermal synthesis. If the C/N mass ratio is intact, so much the better. Subsequently, the MNG hybrids were characterized and employed in the reduction of Nip to Amp, thereby further verifying the activities of *ortho*-carbon atoms next to various N doping mode by the catalytic performance of MNG hybrids. Moreover, the lifetime of MNG nanocatalysts was also evaluated.

## 2. Experimental section

### 2.1. Materials

$\text{FeCl}_3 \cdot 6\text{H}_2\text{O}$  (AR),  $\text{FeCl}_2 \cdot 4\text{H}_2\text{O}$  (AR), and ethylenediamine (AR) were purchased from Tianjin Jiangtian Chemical Co., Ltd., Tianjin, China. Graphite was provided by Tianjin Guangfu Technology Development Co., Ltd., Tianjin, China.  $\text{NdFeB}$  magnet was purchased from Zhengzhou Greatwall Scientific Industrial and Trade Co., Ltd., Zhengzhou, China. Commercially available reagents were used without further purification.

### 2.2. Preparation of magnetic 3D nitrogen doped graphene gels

Graphene oxide (GO) was synthesized by chemical oxidation of graphite according to the Hummer's method [35]. Magnetic 3D nitrogen doped graphene gels (MNG) were prepared by hydrothermal self-assembly of GO, ethylenediamine,  $\text{FeCl}_3 \cdot 6\text{H}_2\text{O}$ , and  $\text{FeCl}_2 \cdot 4\text{H}_2\text{O}$ , followed by freeze-drying. In a typical process, 5 mL solution of  $\text{FeCl}_3 \cdot 6\text{H}_2\text{O}$  (0.081 g) and  $\text{FeCl}_2 \cdot 4\text{H}_2\text{O}$  (0.030 g) was gradually added into 50 mL GO (2 mg/mL) aqueous dispersion. The mixture was sonicated for 10 min to achieve the electrostatic adsorption of Fe (III) and Fe (II) ions on GO, and then 10 mL ethylenediamine was slowly added, sonicated for another 10 min to form a stable suspension. Subsequently, the above suspension was sealed in a 100 mL Teflon-lined autoclave and hydrothermally treated at  $180^\circ\text{C}$  for 12 h. After the autoclave was naturally cooled to room temperature, the hydrogel was taken out by an external magnet, washed with water to neutral and freeze-dried for 24 h to yield the aerogel, designated as MNG-1. (Fig. 1) Moreover, other gels were also prepared by using different amount of  $\text{FeCl}_3 \cdot 6\text{H}_2\text{O}$  and  $\text{FeCl}_2 \cdot 4\text{H}_2\text{O}$ , denoted as MNG-0, MNG-2, and MNG-5, indicating the doses of  $\text{FeCl}_3 \cdot 6\text{H}_2\text{O}$  and  $\text{FeCl}_2 \cdot 4\text{H}_2\text{O}$  are 0, 2, and 5 times of MNG-1, respectively. In the case of MNG-0, 5 mL distilled water was used instead of 5 mL solution of  $\text{FeCl}_3 \cdot 6\text{H}_2\text{O}$  and  $\text{FeCl}_2 \cdot 4\text{H}_2\text{O}$  and MNG-0 was separated by filtration, while other reaction conditions remained unchanged.

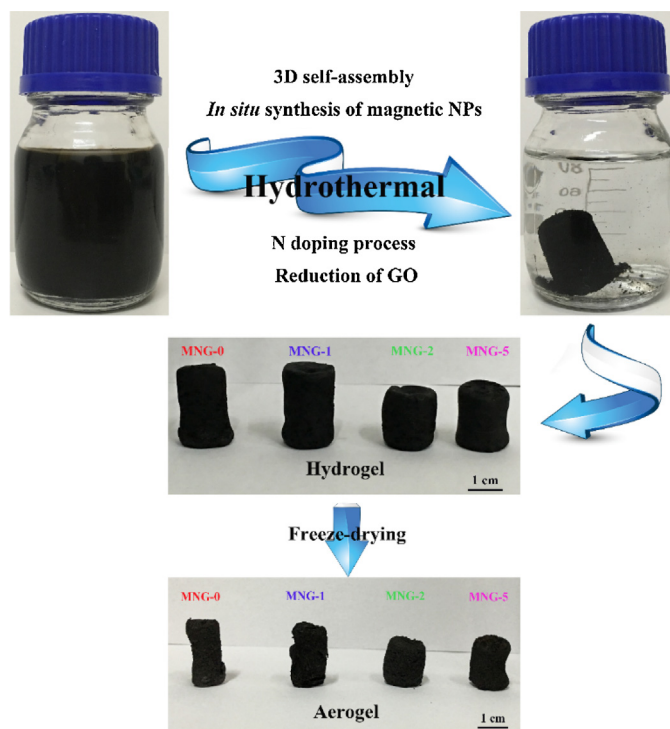


Fig. 1. Fabrication process of MNG hybrids.

### 2.3. Characterization

The X-ray diffraction (XRD) patterns were collected on a Rigaku D/max 2500 using a  $\text{Cu K}\alpha$  X-ray source (40 kV, 100 mA) in the range of  $5\text{--}80^\circ$ . Scanning electron microscopy (SEM) images were recorded on a Hitachi S-4800 microscopy. Transmission electron microscope (TEM) micrographs were obtained with a Tecnai G2 F20 high resolution analytical electron microscope operating at an electron beam voltage of 200 kV. Powder samples were dispersed onto a carbon-coated copper grid for TEM analysis. Magnetization curves were obtained on a LDJ9600-1 superconducting quantum interference device at room temperature. Thermogravimetric analysis (TGA) was determined by a Shimadzu TGA-50 thermogravimetric analyzer from  $25$  to  $750^\circ\text{C}$  with a heating rate of  $10^\circ\text{C}/\text{min}$ . Inductively coupled plasma (ICP) analysis was performed using a Varian Vista-MPX spectrometer. Elemental analysis was carried out on a Vario Micro cube element analyzer. Brunauer-Emmet-Teller (BET) surface areas and pore volumes of the nanocomposites were measured by nitrogen physisorption at a liquid nitrogen temperature on a Micromeritics Tristar II 3020 apparatus. X-ray photoelectron spectroscopy (XPS) was recorded on a PHI1600 spectrometer with a  $\text{Mg K}\alpha$  X-ray source for excitation. UV–vis spectra were obtained on an Evolution 300 UV–vis spectrophotometer.

### 2.3. Catalytic reduction of 4-nitrophenol

The aqueous solution of 4-Nitrophenol (Nip) (0.1 mM, 1.5 mL) was mixed with a freshly prepared  $\text{NaBH}_4$  solution (0.03 M, 1.0 mL). Afterwards, the as-prepared MNG nanocatalysts (1 mg) were added into the reaction mixture. During the reaction process, the yellow-green color became more and more shallow and eventually disappeared. This reaction was monitored by UV–vis spectroscopy. Furthermore, the spent catalysts (MNG-1, MNG-2, and MNG-5) were magnetically separated from the reaction mixture by an external magnet. And then all spent catalysts were washed with distilled water, and reused under the same experimental conditions.

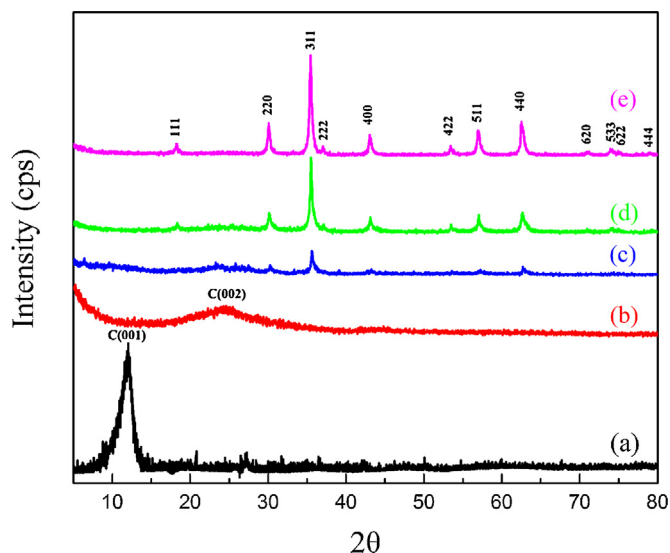


Fig. 2. XRD patterns of GO (a), MNG-0 (b), MNG-1 (c), MNG-2 (d), and MNG-5 (e).

### 3. Results and discussion

The crystal phase and structural properties of the obtained hybrids were characterized by XRD measurements. As shown in Fig. 2, the key indicator of GO at  $11.5^\circ$  was indexed to the (001) plane, corresponding to a 0.77 nm interlayer space, demonstrating the introduction of oxygen-containing groups to form the graphene oxide [36]. In the pattern of MNG-0, this sharp diffraction peak was not present but a new broad reflection at  $24.4^\circ$  was observed, which indexed to the (002) plane of graphite with a spacing of 0.36 nm. These results indicated that GO has been successfully reduced to

graphene [19,37]. In the cases of MNG-1, MNG-2, and MNG-5, reflection peaks at  $18.3^\circ$ ,  $30.1^\circ$ ,  $35.4^\circ$ ,  $37.1^\circ$ ,  $43.1^\circ$ ,  $53.4^\circ$ ,  $56.9^\circ$ ,  $62.5^\circ$ ,  $70.9^\circ$ ,  $74.0^\circ$ ,  $75.0^\circ$ , and  $78.9^\circ$  could be assigned to (111), (220), (311), (222), (400), (422), (511), (440), (620), (533), (622), and (444) crystal faces of  $\text{Fe}_3\text{O}_4$ , respectively. (JCPDS no. 99-0073) Obviously, the XRD patterns confirmed the formation of  $\text{Fe}_3\text{O}_4$  [36,38]. From MNG-0 to MNG-5, it was found that the diffraction peaks of  $\text{Fe}_3\text{O}_4$  were enhanced with increase of  $\text{Fe}_3\text{O}_4$  loading, while the broad reflection at  $24.4^\circ$  decreased gradually and disappeared finally. This regular pattern demonstrated that  $\text{Fe}_3\text{O}_4$  NPs were efficiently deposited on the graphene surface and suppressed the stacking of graphene layers [33]. Moreover, it also could be speculated that the size of  $\text{Fe}_3\text{O}_4$  NPs grew larger with increase of  $\text{Fe}_3\text{O}_4$  loading.

Four MNG materials have been prepared by a one-step hydrothermal reaction and their morphologies were characterized by SEM and TEM. From the SEM images (Fig. 3a–d), all samples presented an interconnected 3D porous network that was rich in hierarchical pores with wide pore size distribution, suggesting efficient assembly during the hydrothermal process. The walls consisted of thin layers of stacked graphene sheets with wrinkled texture. The partially crinkled nature might originate from the defective structures formed during the assembly procedure and the heteroatom doping process [39,40]. TEM was further employed to characterize the nanostructure of MNG composites. Fig. 3e revealed that N-doped graphene layers from MNG-0 were almost transparent with some visible wrinkles, which agreed well with the SEM image. For MNG-1, MNG-2, and MNG-3, numerous NPs were distributed uniformly on the support materials while there was slight aggregation of these NPs with the increase of  $\text{Fe}_3\text{O}_4$  loading, which was caused by the magnetic dipolar interaction among the magnetite NPs [41]. It was notable that the particle size of  $\text{Fe}_3\text{O}_4$  NPs became larger, as its loading increased, and the average particle diameters of MNG-1, MNG-2, and MNG-5 were 8.87,

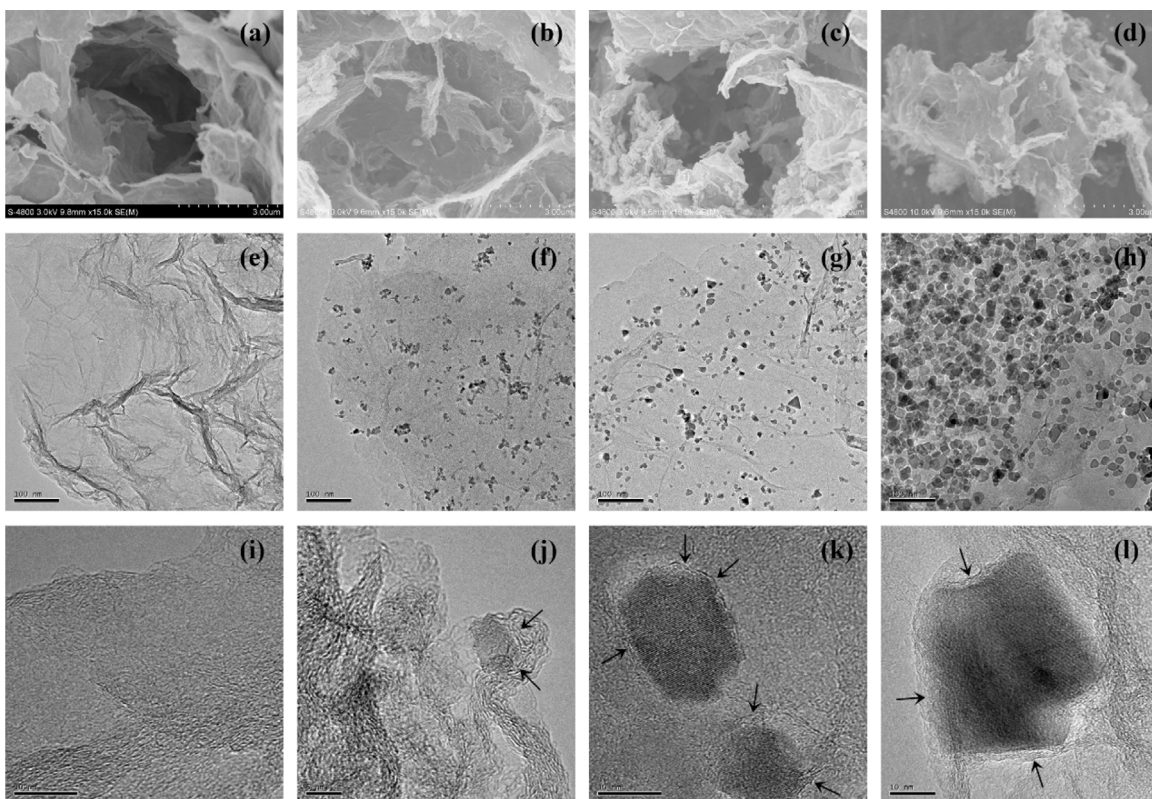
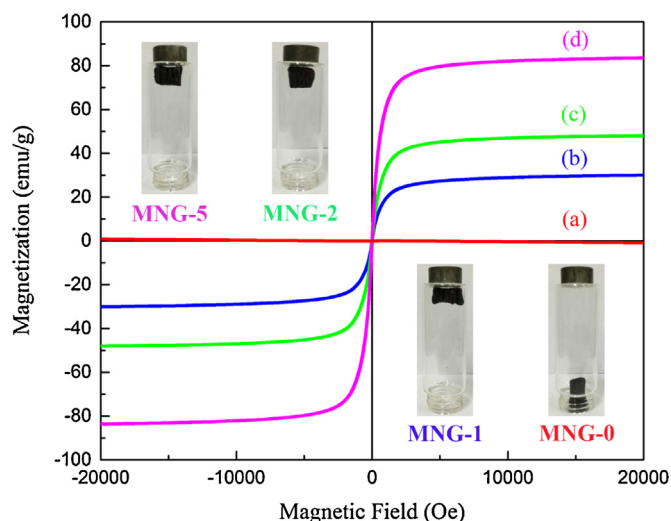


Fig. 3. SEM images of MNG-0 (a), MNG-1(b), MNG-2 (c), and MNG-5 (d); TEM images of MNG-0 (e), MNG-1(f), MNG-2 (g), and MNG-5 (h); HRTEM images of MNG-0 (i), MNG-1(j), MNG-2 (k), and MNG-5 (l).



**Fig. 4.** Magnetization curves of MNG-0 (a), MNG-1 (b), MNG-2 (c), and MNG-5 (d) at 300 K. The insets are the digital photos for the magnetic properties of MNG-0, MNG-1, MNG-2, and MNG-5.

10.88, and 21.91 nm, respectively. (Fig. S1) These results agreed well with XRD characterizations. High-resolution TEM (HRTEM) images showed typical  $\text{Fe}_3\text{O}_4$  NPs with well crystalline textures. Meanwhile, apart from the decoration of  $\text{Fe}_3\text{O}_4$  NPs on both sides of the N-doped graphene sheets (Fig. 3f–h), some of the NPs were embedded or encapsulated in the N-doped graphene layers ( $\leq 7$  layers; Fig. 3j–l), indicating the efficient assembly between NPs and graphene sheets. It is interesting that the embedding or encapsulating can be conducted under hydrothermal reaction, which was traditionally achieved after thermal treatment under drastic conditions [13,33].

The magnetic properties of MNG-0, MNG-1, MNG-2, and MNG-5 were measured in fields between  $-20$  and  $+20$  kOe at ambient temperature (300 K), and the results are summarized in Fig. 4. It was obvious that MNG-0 sample exhibited a diamagnetic response. Except for MNG-0, the obtained magnetization hysteresis loops of MNG-1, MNG-2, and MNG-5 without obvious remanence and coercivity indicated that these three hybrids showed superparamagnetism [42]. This result was consistent with XRD, SEM and TEM characterizations. The specific saturation magnetizations of MNG-1, MNG-2, and MNG-5 were 30.07, 48.04, 83.56 emu/g, respectively, revealing that the saturation magnetization was proportional to  $\text{Fe}_3\text{O}_4$  loading. These high saturation magnetization values facilitated the recycling of these nanocatalysts by a low energy-saving magnetic separation process. In addition, the inserts of Fig. 4 clearly demonstrated that MNG-1, MNG-2, and MNG-5 could be lifted by a magnet even inside a glass vial, indicating the strong interaction between the hybrids and external magnetic field, while MNG-0 could not, which further proved the preceding analyses. In brief, the excellent magnetic response and high saturation magnetization of 3D carbon materials allowed for it to be used in many fields, such as catalysis, bio-sensing, and so on.

The physical and textural properties of all MNG hybrids are summarized in Table 1. The content of Fe was confirmed by TGA (Fig. S2) and ICP-AES. The results obtained by these two methods were very close, and the error was less than 3%. Interestingly, although the loading of  $\text{Fe}_3\text{O}_4$  was near 80%, small amount of GO could still finish the self-assembly process and form the 3D structure. On the basis of elemental analyses, it was obvious that C/N mass ratios of all the samples were almost exactly the same, indicating that the adjustment of magnetic properties did not affect the N doping process. This result is very significant in design and synthesis of MNG materials. Moreover, the BET specific surface, the total pore

volume and average pore diameter of MNG-0, MNG-1, MNG-2, and MNG-5 were detected and the results are also shown in Table 1. It was noteworthy that the BET specific surface area of MNG-1 was higher than that of MNG-0. This result strongly suggested that the  $\text{Fe}_3\text{O}_4$  NPs anchored on the separated graphene surface prevented the graphene sheets from aggregating and restacking [43,44], while the BET specific surface area decreased with the increase of  $\text{Fe}_3\text{O}_4$  loading which was caused by the decrease of graphene content.

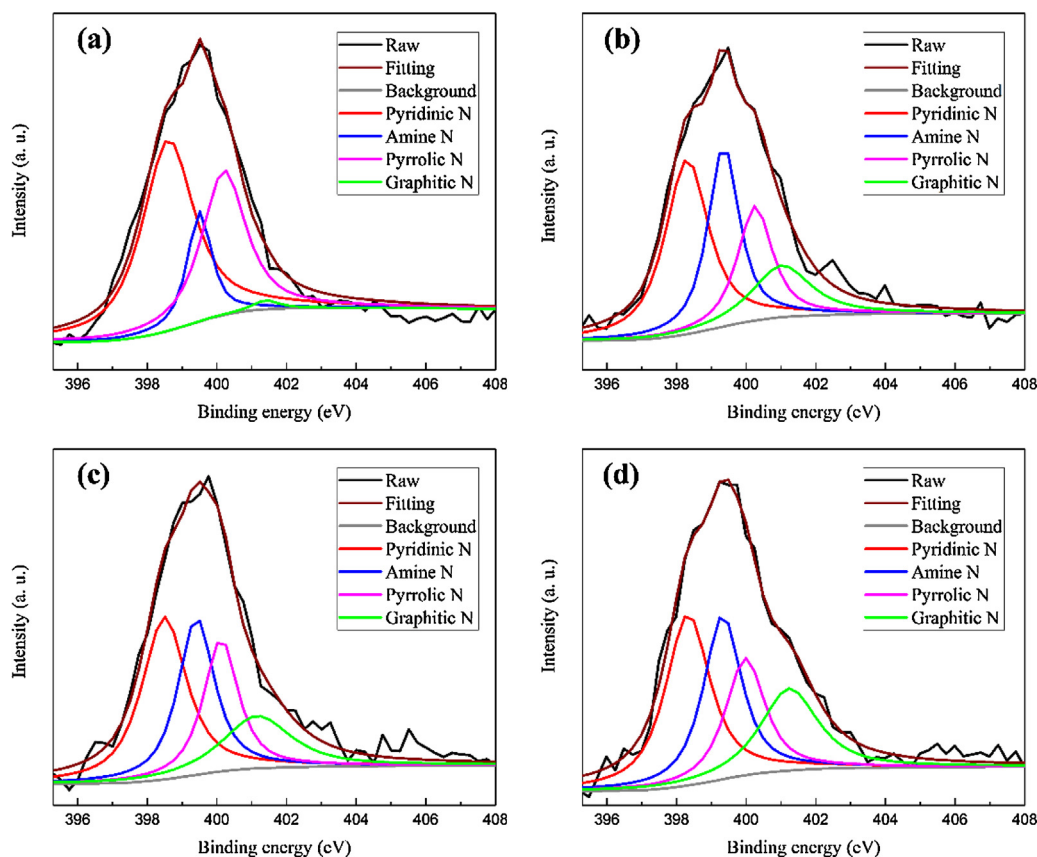
To further confirm the *in situ* synthesis of  $\text{Fe}_3\text{O}_4$  NPs and N doping mode in MNG hybrids, XPS studies have been performed. For MNG-0, there were three peaks in the XPS spectrum, corresponding to C 1s, N 1s, and O 1s at about 284.5, 399.5, and 532.2 eV, respectively (Fig. S3) [14,36]. In comparison with MNG-0, the XPS spectra of MNG-1, MNG-2, and MNG-5 clearly presented two new peaks at about 711.4 eV and 724.9 eV that were characteristic of Fe 2p<sub>3/2</sub> and Fe 2p<sub>1/2</sub> for  $\text{Fe}_3\text{O}_4$ , respectively, confirming the successful decoration of  $\text{Fe}_3\text{O}_4$  NPs in MNG-1, MNG-2, and MNG-5 (Fig. S4) [33,45]. These results were in accordance with the results of XRD and TEM characterizations. The high resolution N 1s XPS spectra of these four hybrids indicated the presence of four kinds of nitrogen, namely, pyridinic N ( $398.5 \pm 0.2$  eV), amino N ( $399.4 \pm 0.2$  eV), pyrrolic N ( $400.2 \pm 0.2$  eV), and graphitic N ( $401.2 \pm 0.2$  eV) [8,12]. All of them have been demonstrated to serve as catalytically active sites for many reactions (Fig. 5) [1,12,14,33,46]. However, different kinds of nitrogen species display different catalytic activities [12,14]. Hence, the relative atomic ratios of each type of nitrogen species are summarized in Table 2 to further understand the N doping mode in these hybrids. According to Fig. 5a and Table 2, the main type of nitrogen was pyridinic N for MNG-0 (51.83% of the total nitrogen atoms), but the content of graphitic N was only 1.2%. As for MNG-1, compared with MNG-0, the compositions of pyridinic N and pyrrolic N decreased sharply, while both amino N and graphitic N increased greatly. In the cases of MNG-2 and MNG-5, the percentages of amino N and pyrrolic N remained about the same by contrast with MNG-1. Nevertheless, the content of pyridinic N continued the downward trend and the percentage of graphitic N kept rising slightly. According to the results of elemental analysis, the C/N mass ratios of these four hybrids were nearly identical. Therefore, it is obvious that the *in situ* synthesis of  $\text{Fe}_3\text{O}_4$  NPs can significantly alter the N doping mode without changing the amount of N doping on graphene layers. Although this kind of change is somewhat restricted, the results are still encouraging. Because the method of regulating N doping mode mentioned by previous reports is to treat NG at high temperatures harshly or replace another nitrogen source tediously. Worse yet, these traditional methods are normally bound to change the total N doping amount. Obviously, the approach of adjusting N doping mode by loading magnetic NPs is more controllable and milder. Moreover, the regulation of N doping mode further causes the change of NG properties, for example, catalytic activity and electrochemical performance.

As mentioned above, the degradation of Nip, which is one of the most extensive phenolic pollutants in waste water is always research focus [11]. Moreover, the degradation product AMP is an important intermediate in the synthesis of various analgesic and antipyretic drugs [47]. So the catalytic performances of MNG nanocatalysts were evaluated by the reduction of Nip with excess  $\text{NaBH}_4$  as a model. UV–vis spectroscopy was used to monitor this reaction. As shown in Fig. 6a, after mixing Nip and  $\text{NaBH}_4$ , an absorption peak at about 400 nm could be observed and the color of the solution appeared yellow or light green due to the formation of Nip ions [47]. After the addition of the nanocatalysts, the peak at about 400 nm decreased whereas the absorption peak at about 300 nm corresponding to AMP increased simultaneously. After a short time, the reaction mixture turned from yellow or green into colorless gradually [48,49]. These phenomena manifested that the reduction of Nip to Amp by  $\text{NaBH}_4$  was successfully catalyzed

**Table 1**

Physical and textural properties of MNG-0, MNG-1, MNG-2, and MNG-5.

Sample	Fe (wt%)		Fe <sub>3</sub> O <sub>4</sub> (wt%)		C/N mass ratio <sup>c</sup>	S <sub>BET</sub> (m <sup>2</sup> /g)	V <sub>total</sub> (cm <sup>3</sup> /g)	D <sub>average</sub> (nm)
MNG-0	–	–	–	–	1/0.11	265.32	0.29	4.73
MNG-1	26.83 <sup>a</sup>	24.78 <sup>b</sup>	37.05 <sup>a</sup>	34.22 <sup>b</sup>	1/0.11	284.03	0.35	4.81
MNG-2	38.66 <sup>a</sup>	36.79 <sup>b</sup>	53.39 <sup>a</sup>	50.81 <sup>b</sup>	1/0.11	178.91	0.34	7.51
MNG-5	55.66 <sup>a</sup>	56.41 <sup>b</sup>	76.87 <sup>a</sup>	77.90 <sup>b</sup>	1/0.10	94.80	0.24	9.05

<sup>a</sup> Calculated by TGA.<sup>b</sup> Measured by ICP-AES.<sup>c</sup> Measured by elemental analysis.**Fig. 5.** High-resolution XPS spectra of the N 1s region for MNG-0 (a), MNG-1 (b), MNG-2 (c), and MNG-5 (d).**Table 2**

The peak positions and relative atomic compositions of nitrogen species for MNG-0, MNG-1, MNG-2, MNG-5 samples based on XPS analysis.

Sample	Pyridinic N		Amine N		Pyrrolic N		Graphitic N	
	BE (eV)	Ratio (%)	BE (eV)	Ratio (%)	BE (eV)	Ratio (%)	BE (eV)	Ratio (%)
MNG-0	398.6	51.83	399.5	13.93	400.2	33.04	401.4	1.20
MNG-1	398.3	37.62	399.4	27.88	400.3	19.56	401.0	14.94
MNG-2	398.5	34.53	399.4	26.86	400.1	21.71	401.2	16.90
MNG-5	398.3	32.98	399.3	26.94	400.0	19.88	401.2	20.20

by MNG nanocatalysts. Furthermore, a controlled experiment was also performed [27]. The adsorption capacity of the material to 4-nitrophenol without NaBH<sub>4</sub> was evaluated (Fig. S5). It was hard for catalytic dosages of MNG nanocatalysts to adsorb 4-nitrophenol completely in 20 min. However, in the presence of NaBH<sub>4</sub>, small doses of MNG could efficiently catalyzed the degradation of 4-nitrophenol in a short time.

From Fig. 6b, it was clear that the reduction reaction did not occur without catalyst, demonstrating MNG catalysts play an important role in this reaction. The induction time  $t_0$  was attributed to the initial adsorption of Nip ions at the active sites on the catalyst [12,49]. Generally, the catalytic reduction of

4-nitrophenol over metallic catalysts is a pseudo-first-order reaction [18,22,27,28,42,49], while N-doped graphene leads to the pseudo-zero-order reaction due to the limited number of active sites. Moreover, there are so many factors that can influence the catalytic performance of this metal-free catalyst, such as N doping amount, N doping mode and so on [12,14]. As shown in Fig. 6b, the absorbance intensity of UV-vis spectroscopy changed linearly with time for MNG-0 catalyzed reaction, indicating pseudo-zero-order kinetics ( $k = 5.74 \times 10^{-8} \text{ mol} \cdot \text{L}^{-1} \cdot \text{s}^{-1}$ ), which confirmed the metal-free catalyst for this reaction [12]. According to Fig. 6b, the catalytic abilities were different among the MNG nanocatalysts in order: MNG-1 > MNG-2 > MNG-5 > MNG-0. It was worth noting that the

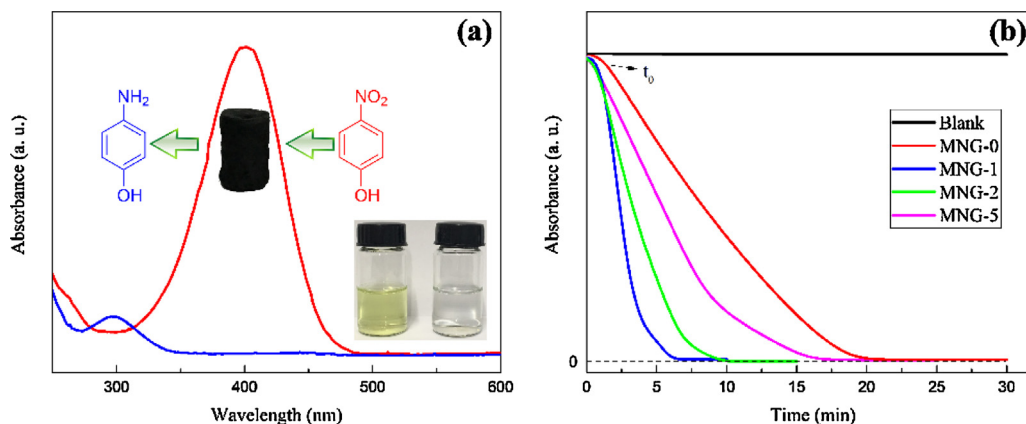


**Fig. 6.** UV-vis spectra of 4-nitrophenol reduction reaction in the absence and presence of MNG nanocatalysts (a). Time curves of the absorbance at 400 nm measured for MNG nanocatalysts (b).

catalytic activities of MNG-1, MNG-2, and MNG-5 were much higher than MNG-0. As is well known,  $\text{Fe}_3\text{O}_4$  NPs themselves almost exhibited no catalytic activity for this reaction at room temperature [42]. Therefore, the enhancement of MNG catalytic activities was possibly attributed to the change of N doping forms: the rising levels of amino N and graphitic N, rather than the specific surface area [1]. The experimental observation agreed well with the afore-said speculation: the carbon atoms next to amino N and graphitic N exhibited higher catalytic activity than those next to pyridinic N and pyrrolic N. Meanwhile, for MNG-1, MNG-2, and MNG-5, catalytic activities decreased accordingly due to the obvious drop of N-doped graphene amount in the catalyst. Furthermore, it was interesting that the reaction catalyzed by these three catalysts did not follow the pseudo-zero-order kinetics in the terminal stage, and there were inflections on the last portion of their absorbance-time curves of 400 nm, which were apparently different from that of MNG-0. Although the reaction process is too complicated to be clearly elucidated, it is speculated that during initial and mid stages of the reduction, the catalytic reduction using MNG-1, MNG-2, and MNG-5 is a pseudo-zero-order reaction ( $k = 3.09 \times 10^{-7} \text{ mol}\cdot\text{L}^{-1}\cdot\text{s}^{-1}$ ,  $1.62 \times 10^{-7} \text{ mol}\cdot\text{L}^{-1}\cdot\text{s}^{-1}$ , and  $8.87 \times 10^{-8} \text{ mol}\cdot\text{L}^{-1}\cdot\text{s}^{-1}$ , respectively) due to the limited number of active sites which is the key factor to control the reaction speed rather than the concentration of the reactant. However, when Nip concentration decreases to a certain degree as the reaction progress, it becomes to be another important controlling factor of this reaction speed. Obviously, the *in situ* synthesis of  $\text{Fe}_3\text{O}_4$  NPs on graphene can indeed enhance the catalytic activity of MNG nanocatalysts by changing N doping forms without altering the C/N mass ratio. Moreover, as shown in Fig. 7, it could be found that MNG-1, MNG-2, and MNG-5 exhibited excellent stability, which could be recycled at least five times with no deactivation in the catalytic performance. There was no significant change of their morphology before and after 5 cycles (Fig. S6). This might be because the nanocatalysts were washed by distilled water after each run. Meanwhile, it was speculated that the 3D graphene framework prevented  $\text{Fe}_3\text{O}_4$  nanoparticles from leakage and being washed away, indicating the synergistic effect of graphene and  $\text{Fe}_3\text{O}_4$  nanoparticles.

#### 4. Conclusion

Four MNG hybrids were easily synthesized *via* a convenient one-pot hydrothermal process. It was found that N doping process, reduction of graphene oxide and  $\text{Fe}_3\text{O}_4$  nanoparticles (NPs) generation *in situ* proceeded simultaneously, accompanied by the three-dimensional self-assembly. SEM and TEM characterizations indicated that these composites exhibited interconnected

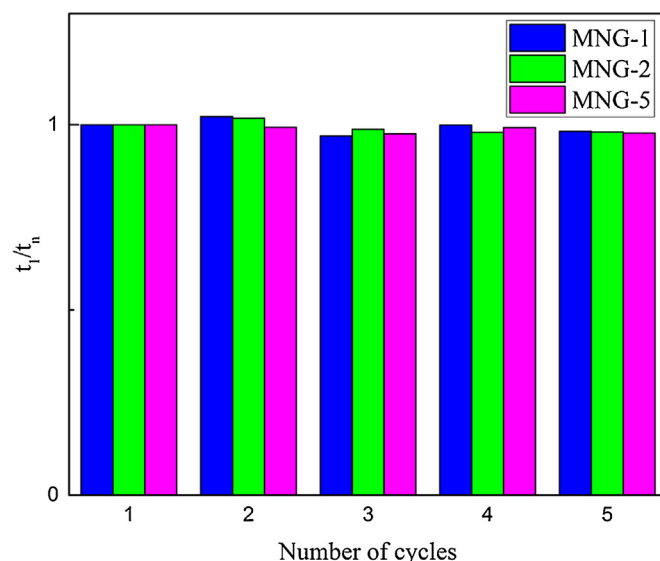


**Fig. 7.** Normalized reaction time at different cycles of the reduction of Nip to Amp using MNG-1, MNG-2, and MNG-5.

poriferous frameworks of graphene sheets with uniform dispersion of  $\text{Fe}_3\text{O}_4$  NPs embedded or encapsulated in the N-doped graphene layers. The results of XRD and XPS demonstrated the *in situ* synthesis of  $\text{Fe}_3\text{O}_4$  NPs which endowed the hybrids magnetic performance. The details of physical and textural properties of all MNG hybrids were also studied. It was shown that the  $\text{Fe}_3\text{O}_4$  NPs anchored on the separated graphene surface prevented the graphene sheets from aggregating and restacking. And even with extremely high levels of  $\text{Fe}_3\text{O}_4$ , tiny amount of GO could still finish the self-assembly process and form the 3D structure. Moreover, XPS characterization further confirmed that the *in situ* synthesis of  $\text{Fe}_3\text{O}_4$  NPs could significantly alter the N doping mode without changing the C/N mass ratio in graphene layers, and result in higher level of amino N and graphitic N, which was different from thermal treatment at high temperatures mentioned by previous reports. At last, the catalytic performances of MNG nanocatalysts were evaluated by the reduction of Nip to Amp. The results indicated that the catalytic activity of MNG hybrids with  $\text{Fe}_3\text{O}_4$  NPs loading was much higher than that without them due to the change of N doping mode, as well as the reaction no longer simply followed the pseudo-zero-order kinetics in final stage. This might be attributed to the enhancement of catalytic activity. Furthermore, MNG nanocatalysts could be easily recycled by virtue of their

superparamagnetism and efficiently used for at least five cycles with no significant decrease in activity. Obviously, MNG hybrids show potential applicative value in many fields, such as catalysis, electrochemistry, and so on.

## Acknowledgements

Financial support was provided by the National Natural Science Foundation of China (Grant No. 21576194).

## Appendix A. Supplementary data

Supplementary data associated with this article can be found, in the online version, at <http://dx.doi.org/10.1016/j.apcatb.2016.11.042>.

## References

- [1] Y. Gao, G. Hu, J. Zhong, Z. Shi, Y. Zhu, D.S. Su, J. Wang, X. Bao, D. Ma, Nitrogen-doped  $sp^2$ -hybridized carbon as a superior catalyst for selective oxidation, *Angew. Chem. Int. Ed.* 52 (2013) 2109–2113.
- [2] X. Kong, Q. Chen, Z. Sun, Enhanced oxygen reduction reactions in fuel cells on H-decorated and B-substituted graphene, *ChemPhysChem* 14 (2013) 514–519.
- [3] Y. Li, Y. Zhao, H. Cheng, Y. Hu, G. Shi, L. Dai, L. Qu, Nitrogen-doped graphene quantum dots with oxygen-rich functional groups, *J. Am. Chem. Soc.* 134 (2011) 15–18.
- [4] A. Pendashteh, J. Palma, M. Anderson, R. Marcilla, NiCoMnO<sub>4</sub> nanoparticles on N-doped graphene: highly efficient bifunctional electrocatalyst for oxygen reduction/evolution reactions, *Appl. Catal. B: Environ.* 201 (2017) 241–252.
- [5] R. Nie, M. Miao, W. Du, J. Shi, Y. Liu, Z. Hou, Selective hydrogenation of C=C bond over N-doped reduced graphene oxides supported Pd catalyst, *Appl. Catal. B: Environ.* 180 (2016) 607–613.
- [6] H. Zhang, Y. Chen, M. Liang, L. Xu, S. Qi, H. Chen, X. Chen, Solid-phase synthesis of highly fluorescent nitrogen-doped carbon dots for sensitive and selective probing ferric ions in living cells, *Anal. Chem.* 86 (2014) 9846–9852.
- [7] Z. Yue, A. Liu, C. Zhang, J. Huang, M. Zhu, Y. Du, P. Yang, Noble-metal-free hetero-structural CdS/Nb<sub>2</sub>O<sub>5</sub>/N-doped-graphene ternary photocatalytic system as visible-light-driven photocatalyst for hydrogen evolution, *Appl. Catal. B: Environ.* 201 (2017) 202–210.
- [8] P. Chen, J. Yang, S. Li, Z. Wang, T. Xiao, Y. Qian, S. Yu, Hydrothermal synthesis of macroscopic nitrogen-doped graphene hydrogels for ultrafast supercapacitor, *Nano Energy* 2 (2013) 249–256.
- [9] F. Jaouen, J. Herranz, M. Lefèvre, J. Dodelet, U.I. Kramm, I. Herrmann, P. Bogdanoff, J. Maruyama, T. Nagaoka, A. Garsuch, J.R. Dahn, T. Olson, S. Pylypenko, P. Atanassov, E.A. Ustinov, Cross-laboratory experimental study of non-noble-metal electrocatalysts for the oxygen reduction reaction, *ACS Appl. Mater. Interfaces* 1 (2009) 1623–1639.
- [10] R. Arrigo, M. Haevecker, S. Wrabetz, R. Blume, M. Lerch, J. McGregor, E.P.J. Parrott, J.A. Zeitler, L.F. Gladden, A. Knop-Gericke, R. Schlögl, D.S. Su, Tuning the acid/base properties of nanocarbons by functionalization via amination, *J. Am. Chem. Soc.* 132 (2010) 9616–9630.
- [11] M. Nemanashi, R. Meijboom, Synthesis and characterization of Cu, Ag and Au dendrimer-encapsulated nanoparticles and their application in the reduction of 4-nitrophenol to 4-aminophenol, *J. Colloid Interface Sci.* 389 (2013) 260–267.
- [12] X. Kong, Z. Sun, M. Chen, C. Chen, Q. Chen, Metal-free catalytic reduction of 4-nitrophenol to 4-aminophenol by N-doped graphene, *Energy Environ. Sci.* 6 (2013) 3260–3266.
- [13] R.V. Jagadeesh, A.-E. Surkus, H. Junge, M.-M. Pohl, J. Rabeah, H. Huan, V. Schünemann, A. Brückner, M. Beller, Nanoscale Fe<sub>2</sub>O<sub>3</sub>-based catalysts for selective hydrogenation of nitroarenes to anilines, *Science* 342 (2013) 1073–1076.
- [14] F. Yang, C. Chi, C. Wang, Y. Wang, Y. Li, High graphite N content in nitrogen-doped graphene as an efficient metal-free catalyst for reduction of nitroarenes in water, *Green Chem.* 18 (2016) 4254–4262.
- [15] D. Long, W. Li, L. Ling, J. Miyawaki, I. Mochida, S.-H. Yoon, Preparation of nitrogen-doped graphene sheets by a combined chemical and hydrothermal reduction of graphene oxide, *Langmuir* 26 (2010) 16096–16102.
- [16] H. Cong, X. Ren, P. Wang, S. Yu, Macroscopic multifunctional graphene-based hydrogels and aerogels by a metal ion induced self-assembly process, *ACS Nano* 6 (2012) 2693–2703.
- [17] X. Yuan, H. Xin, X. Qin, X. Li, Y. Liu, H. Guo, Self-assembly of SiO<sub>2</sub>/reduced graphene oxide composite as high-performance anode materials for Li-ion batteries, *Electrochim. Acta* 155 (2015) 251–256.
- [18] J. Luo, N. Zhang, J. Lai, R. Liu, X. Liu, Tannic acid functionalized graphene hydrogel for entrapping gold nanoparticles with high catalytic performance toward dye reduction, *J. Hazard. Mater.* 300 (2015) 615–623.
- [19] L. Guo, P. Ye, J. Wang, F. Fu, Z. Wu, Three-dimensional Fe<sub>3</sub>O<sub>4</sub>-graphene macroscopic composites for arsenic and arsenate removal, *J. Hazard. Mater.* 298 (2015) 28–35.
- [20] X. Zheng, Q. Zhu, H. Song, X. Zhao, T. Yi, H. Chen, X. Chen, *In situ* synthesis of self-assembled three-dimensional graphene-magnetic palladium nanohybrids with dual-enzyme activity through one-pot strategy and its application in glucose probe, *ACS Appl. Mater. Interfaces* 7 (2015) 3480–3491.
- [21] M. Nawaz, W. Miran, J. Jang, D.S. Lee, One-step hydrothermal synthesis of porous 3D reduced graphene oxide/TiO<sub>2</sub> aerogel for carbamazepine photodegradation in aqueous solution, *Appl. Catal. B: Environ.* 203 (2017) 85–95.
- [22] J. Li, C. Liu, Y. Liu, Au/graphene hydrogel: synthesis, characterization and its use for catalytic reduction of 4-nitrophenol, *J. Mater. Chem.* 22 (2012) 8426–8430.
- [23] Z. Zhang, T. Sun, C. Chen, F. Xiao, Z. Gong, S. Wang, Bifunctional nanocatalyst based on three-dimensional carbon nanotube-graphene hydrogel supported Pd nanoparticles: one-pot synthesis and its catalytic properties, *ACS Appl. Mater. Interfaces* 6 (2014) 21035–21040.
- [24] B. Wang, W. Fang, L. Si, Y. Li, X. Yan, L. Chen, S. Wang, Construction of 2-(2'-hydroxy-5'-methylphenyl) benzotriazole over Pd/γ-Al<sub>2</sub>O<sub>3</sub> by a continuous process, *ACS Sustainable Chem. Eng.* 3 (2015) 1890–1896.
- [25] S. Chappa, A.M. Mhatre, V.C. Adya, A.K. Pandey, Egg-shell membrane mimicking synthetic polymer membrane supported palladium nanoparticles for catalyzing reduction of uranyl(VI) ions, *Appl. Catal. B: Environ.* 203 (2017) 53–64.
- [26] B. Wang, L. Si, Y. Yuan, Y. Li, L. Chen, X. Yan, Reductive cyclization of 2-nitro-2'-hydroxy-5'-methylazobenzene to benzotriazole over K-doped Pd/γ-Al<sub>2</sub>O<sub>3</sub>, *RSC Adv.* 6 (2016) 16766–16771.
- [27] W. Ye, J. Yu, Y. Zhou, D. Gao, D. Wang, C. Wang, D. Xue, Green synthesis of Pt-Au dendrimer-like nanoparticles supported on polydopamine-functionalized graphene and their high performance toward 4-nitrophenol reduction, *Appl. Catal. B: Environ.* 181 (2016) 371–378.
- [28] W. Zhang, Y. Sun, L. Zhang, *In situ* synthesis of monodisperse silver nanoparticles on sulfhydryl-functionalized poly(glycidyl methacrylate) microspheres for catalytic reduction of 4-nitrophenol, *Ind. Eng. Chem. Res.* 54 (2015) 6480–6488.
- [29] W. Ye, Y. Chen, Y. Zhou, J. Fu, W. Wu, D. Gao, F. Zhou, C. Wang, D. Xue, Enhancing the catalytic activity of flowerlike Pt nanocrystals using polydopamine functionalized graphene supports for methanol electrooxidation, *Electrochim. Acta* 142 (2014) 18–24.
- [30] S.-W. Kim, M. Park, H. Kim, K.J. Yoon, J.-W. Son, J.-H. Lee, B.-K. Kim, J.-H. Lee, J. Hong, *In-situ* nano-alloying Pd-Ni for economical control of syngas production from high-temperature thermo-electrochemical reduction of steam/CO<sub>2</sub>, *Appl. Catal. B: Environ.* 200 (2017) 265–273.
- [31] W. Ye, X. Shi, J. Su, Y. Chen, J. Fu, X. Zhao, F. Zhou, C. Wang, D. Xue, One-step reduction and functionalization protocol to synthesize polydopamine wrapping Ag/graphene hybrid for efficient oxidation of hydroquinone to benzoquinone, *Appl. Catal. B: Environ.* 160–161 (2014) 400–407.
- [32] H. Liu, J. Wang, Z. Feng, Y. Lin, L. Zhang, D. Su, Facile synthesis of Au nanoparticles embedded in an ultrathin hollow graphene nanoshell with robust catalytic performance, *Small* 11 (2015) 5059–5064.
- [33] Z.-S. Wu, S. Yang, Y. Sun, K. Parvez, S. Feng, K. Müllen, 3D nitrogen-doped graphene aerogel-supported Fe<sub>3</sub>O<sub>4</sub> nanoparticles as efficient electrocatalysts for the oxygen reduction reaction, *J. Am. Chem. Soc.* 134 (2012) 9082–9085.
- [34] T. He, Z. Li, Z. Sun, S. Chen, R. Shen, L. Yi, L. Deng, M. Yang, H. Liu, Y. Zhang, From supramolecular hydrogels to functional aerogels: a facile strategy to fabricate Fe<sub>3</sub>O<sub>4</sub>/N-doped graphene composites, *RSC Adv.* 5 (2015) 77296–77302.
- [35] W.S. Hummers, R.E. Offeman, Preparation of graphitic oxide, *J. Am. Chem. Soc.* 80 (1958) 1339–1339.
- [36] H. Hu, Z. Zhao, W. Wan, Y. Gogotsi, J. Qiu, Ultralight and highly compressible graphene aerogels, *Adv. Mater.* 25 (2013) 2219–2223.
- [37] W. Chen, S. Li, C. Chen, L. Yan, Self-assembly and embedding of nanoparticles by *in situ* reduced graphene for preparation of a 3D graphene/nanoparticle aerogel, *Adv. Mater.* 23 (2011) 5679–5683.
- [38] E. Pardieu, S. Pronkin, M. Dolci, T. Dintzer, B.P. Pichon, D. Begin, C. Pham-Huu, P. Schaaf, S. Begin-Colin, F. Boulmedais, Hybrid layer-by-layer composites based on a conducting polyelectrolyte and Fe<sub>3</sub>O<sub>4</sub> nanostructures grafted onto graphene for supercapacitor application, *J. Mater. Chem. A* 3 (2015) 22877–22885.
- [39] Y. Su, Y. Zhang, X. Zhuang, S. Li, D. Wu, F. Zhang, X. Feng, Low-temperature synthesis of nitrogen/sulfur co-doped three-dimensional graphene frameworks as efficient metal-free electrocatalyst for oxygen reduction reaction, *Carbon* 62 (2013) 296–301.
- [40] S. Yang, L. Zhi, K. Tang, X. Feng, J. Maier, K. Müllen, Efficient synthesis of heteroatom (N or S)-doped graphene based on ultrathin graphene oxide-porous silica sheets for oxygen reduction reactions, *Adv. Funct. Mater.* 22 (2012) 3634–3640.
- [41] Y. Yao, S. Miao, S. Liu, L.P. Ma, H. Sun, S. Wang, Synthesis characterization, and adsorption properties of magnetic Fe<sub>3</sub>O<sub>4</sub>@ graphene nanocomposite, *Chem. Eng. J.* 184 (2012) 326–332.
- [42] W. Gu, X. Deng, X. Jia, J. Li, E. Wang, Functionalized graphene/Fe<sub>3</sub>O<sub>4</sub> supported AuPt alloy as a magnetic, stable and recyclable catalyst for a catalytic reduction reaction, *J. Mater. Chem. A* 3 (2015) 8793–8799.
- [43] H. Wang, Z. Xu, H. Yi, H. Wei, Z. Guo, X. Wang, One-step preparation of single-crystalline Fe<sub>2</sub>O<sub>3</sub> particles/graphene composite hydrogels as high

- performance anode materials for supercapacitors, *Nano Energy* 7 (2014) 86–96.
- [44] Y. Si, E.T. Samulski, Exfoliated graphene separated by platinum nanoparticles, *Chem. Mater.* 20 (2008) 6792–6797.
- [45] J. Jiao, W. Qiu, J. Tang, L. Chen, L. Jing, Synthesis of well-defined  $\text{Fe}_3\text{O}_4$  nanorods/N-doped graphene for lithium-ion batteries, *Nano Res.* 9 (2016) 1256–1266.
- [46] K. Gong, F. Du, Z. Xia, M. Durstock, L. Dai, Nitrogen-doped carbon nanotube arrays with high electrocatalytic activity for oxygen reduction, *Science* 323 (2009) 760–764.
- [47] L. Han, C. Zhu, L. Wang, S. Dong, Facile synthesis of chain-like CoCu bimetallic nanomaterials and their catalytic properties, *Catal. Sci. Technol.* 3 (2013) 1501–1504.
- [48] P. Herve, M. Pérez-Lorenzo, L.M. Liz-Marzan, J. Dzubiella, Y. Lu, M. Ballauff, Catalysis by metallic nanoparticles in aqueous solution: model reactions, *Chem. Soc. Rev.* 41 (2012) 5577–5587.
- [49] S. Wunder, F. Polzer, Y. Lu, Y. Mei, M. Ballauff, Kinetic analysis of catalytic reduction of 4-nitrophenol by metallic nanoparticles immobilized in spherical polyelectrolyte brushes, *J. Phys. Chem. C* 114 (2010) 8814–8820.